Magnetic Field Energy Harvesting under Overhead Power Lines

Sheng Yuan, Yi Huang, *Senior Member, IEEE*, Jiafeng Zhou, Qian Xu, Chaoyun Song and Pete Thompson

Abstract—**Condition monitoring for overhead power lines is critical for power transmission networks to improve their reliability, detect potential problems in the early stage and ensure the utilization of the transmitting full capacity. Energy harvesting can be an effective solution for autonomous, self-powered wireless sensors. In this paper, a novel bow-tie-shaped coil is proposed which is placed directly under overhead power lines to scavenge the magnetic field energy. Compared to the conventional method by mounting the energy harvester on the power lines, this approach provides more flexibility and space to power bigger sensors such as the weather station. As the harvesting coil cannot entirely enclose the power lines, the demagnetization factor which is closely related to the core geometry should be considered and optimized. We therefore design a new bow-tie-shaped core that can have a much lower demagnetization factor (hence more power) than that of the conventional solenoid. The selection of core material is studied and found that Mn-Zn ferrite is the most suitable core material because it greatly reduces the eddy current losses and also has high permeability. Experiment results show that the bow-tie coil could have a power density of 1.86 μW/cm^3 when placed in a magnetic flux density of 7 μT$_{rms}$. This value is 15 times greater than the reported results under the same condition. If a longer bow-tie coil with more turns is placed in a magnetic flux density of 11 μT$_{rms}$, the produced power density is 103.5 μW/cm^3 which is comparable to a solar panel working during a cloudy day. Thus the proposed solution is a very efficient and attractive method for harvesting the magnetic field energy for a range of monitoring applications.**

Index Terms— **Energy harvesting, overhead power line, condition monitoring, inductive coil.**

I. INTRODUCTION

For electric power transmission networks, high voltage overhead power lines are of great importance. Due to temperature variations, aging effects and ice accumulation [1, 2], the sag of the conductor may lead to dangerous circumstances and huge maintenance costs [3]. Hence, monitoring overhead power line conditions, disturbances, faults and sags is essential to ensure the proper operation of the power line transmission networks. Several critical parameters such as the ambient temperature and the line current may affect the operability and availability of overhead power lines. With the advancement in wireless communication technologies, inexpensive and ultra-low power wireless sensors have been developed and can be applied to monitoring these important parameters. However, the finite life span of the batteries which power the sensing system becomes a bottleneck as it is expensive to periodically replace these batteries. Thus, the energy harvesting technology is an attractive and promising solution to make the system monitoring self-sustainable [4].

There are several ambient energy sources (solar, wind, electromagnetic, etc.). Solar panels are a good option to collect energy during daytime in good weather conditions [4, 5]. This technology is relatively mature and many products are already available on the market. However, a solar energy device heavily relies on weather conditions and may require additional high-capacity energy storage units which are normally expensive in order to work at night [3, 6]. Similar situations apply to the small wind turbine. Furthermore, harsh weather conditions like hail and storms could damage the turbine blades and solar panels [3, 7]. In the vicinity of high voltage power lines, a strong electromagnetic field is generated, which could be a consistent energy source for wireless sensors. Recently, a number of energy harvesting devices have been developed to collect the electrical [3, 8-12] or magnetic field energy from overhead power lines [13-17]. These devices are all wrapped on the power lines as shown in Fig. 1 to provide a range of wireless measurements such as conductor temperature, line sags and ambient temperature.

A limitation of all these designs is that the devices have to be mounted on overhead power lines. This limits the size and the weight of the sensors as it would further increase the line sag. The real-time weather data (such as wind speed, humidity and air temperature) near overhead power lines is the foundation of
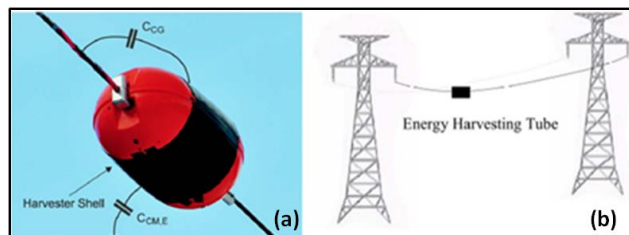
Fig. 1. Energy harvesters mounted on the overhead power line. (a) from [10] and (b) from [11]

the dynamic thermal rating technique, which could have a significant increase in the transmission capacity compared with the traditional static rating [18, 19]. Normally, the size of a weather station with a wind sensor is relatively large compared with temperature and humidity sensors [20]. Besides, it needs to be installed on a stationary object to keep it still. Therefore it is almost impractical to connect the weather station to a conventional energy harvester which is mounted on the power line. An energy harvesting device placed off the power lines, such as on the ground shown in Fig. 2 can overcome these short comings. Besides, this free-standing energy harvester can be easily combined with the solar pane or the wind turbine to form a reliable and efficient energy harvesting system. Zhu and colleagues designed a free standing capacitor to scavenge the electric field energy in a substation [21, 22]. However, the power output was limited due to the loading effect caused by the large impedance of the capacitor. Tashiro *et al* used Brooks coils to harvest the energy from the power line [15]. From their experiment, a power density of 1.47 $\mu W/cm^3$ was achieved in an area with the magnetic flux density of 21.2 μT_{rms}. Their power density was limited due to the core shape and material. Roscoe *et al* designed a 50 cm long solenoid with a diameter of 5 cm to collect the magnetic field energy in a substation [23]. The power density in the coil was 0.845 $\mu W/cm^3$ when it was placed in a field of magnetic flux density of 18.5 μT_{rms}. They selected cast iron as the coil core material which suffered greatly from the eddy current losses. This paper provides a comprehensive study on the magnetic field energy harvester in terms of the coil geometrical shape, core material and winding method. In Section II, the magnetic flux density under the power lines is investigated. Details on the coil designs and design equations are given in Section III. In Section IV, the experiment evaluation of the proposed designs is presented. The discussion and conclusions are given in Section V and Section VI, respectively.

II. MAGNETIC FLUX DENSITY UNDER POWER LINES

There are several published papers on the investigation of the levels of the magnetic flux density *B* under overhead power lines. They have confirmed that the flux density does not
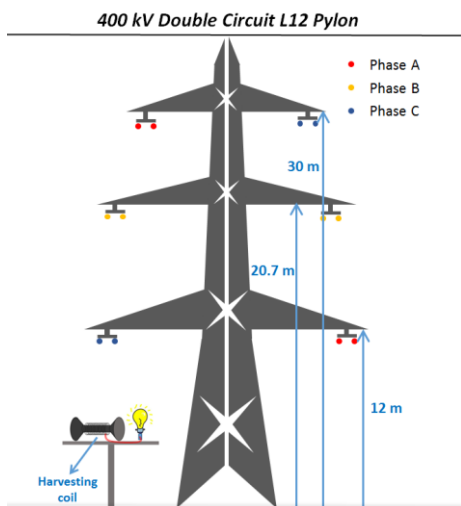

Fig. 2. The physical structure of the 400 kV double circuit L12 pylon

exceed regulatory levels near the ground [25-28]. Obviously, for different kinds of pylons, the physical structures of overhead power lines and their corresponding typical line currents are different, resulting in various magnetic flux densities. The National Grid in the UK has conducted an in-depth research on the average magnetic flux density under various pylons [29]. In addition to the current, the magnetic flux density is also affected by some external factors such as the air humidity [30], line sag [31] and unbalanced three-phase current [32, 33]. The magnetic flux density under overhead power lines can vary greatly from time to time. Thus, the average measurement result is more meaningful. The National Grid has provided an average value of the magnetic flux density under the 400 kV L12 overhead power lines [29]. Their measurement results are shown in Fig. 3. The magnetic flux density decreases as the horizontal distance from the centerline of overhead power conductors increases. When the measurement height is 1 m above the ground, the magnetic flux density is around 6 μT_{rms}.
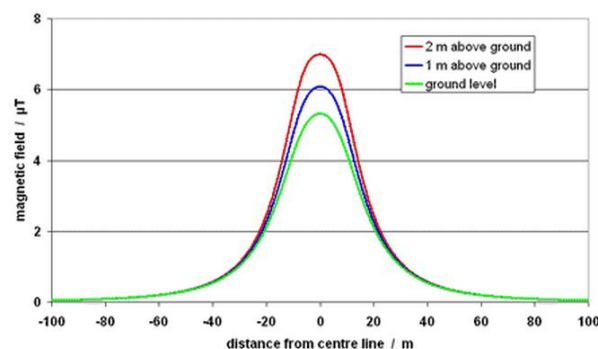

Fig. 3. The distribution of the magnetic flux density under 400 kV double circuit overhead power lines [29].

III. THE ENERGY HARVESTER DESIGN

A. System Modelling

At 50 Hz, the most efficient way to harvest the magnetic energy is to employ coils wrapped typically on ferromagnetic cores. Though the energy harvesting coil may be more than 10 meters away from the overhead power lines, it is still an inductive coupling system since the wavelength of the 50 Hz electromagnetic wave is extremely long. Therefore, the maximum power that the coil can harvest does not solely depend on the surrounding magnetic field, but also on such as the effective coil resistance and the optimized load. Fig. 4 shows the equivalent circuit of a harvesting coil connected with
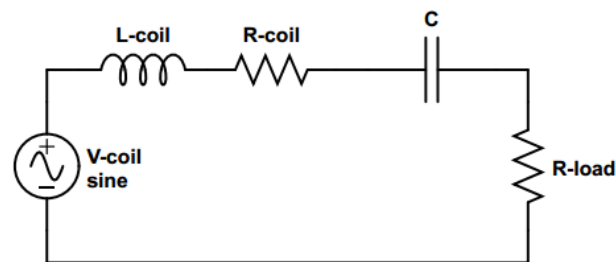

Fig. 4. The equivalent circuit of the harvesting coil with a matched load. A compensating capacitor *C* is added to eliminate the coil inductance *L-coil*. The load resistor *R-load* is selected to have the same value as the coil resistance *R-coil*.
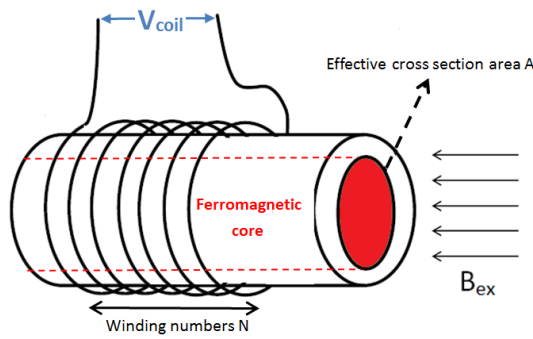
Fig. 5. Coil voltage generation by applying alternating magnetic flux modified from [23]

a compensating capacitor and a load resistor with the same value of R_{coil}. The induced coil voltage V_{coil} is a function of the surrounding magnetic flux density and the coil properties by applying Faraday's Law:

$$V_{coil} = N\omega B_{ex}A\mu_{eff} \qquad (1)$$

where V_{coil} is the peak value of the AC waveform, N is the number of turns winding on the coil, B_{ex} is the external magnetic flux density in T applied to the coil, A represents the effective cross section of the coil in m^2, ω is the angular frequency in rad/s and μ_{eff} is the effective permeability related to the core material and core geometry.

The effective coil resistance R_{coil} consists of two parts: copper resistance and equivalent core resistance. The copper resistance is caused by the resistance of the long enameled wire winding on the core.

$$R_{copper} = \rho l_{wire} \qquad (2)$$

where ρ is the resistivity of the copper wire in Ω/m and l_{wire} is the total length of the enameled wire in m. When the core is subject to a time-varying magnetic field, some of the power to be delivered to the load is lost in the core and is dissipated as heat. These losses can be treated as the equivalent core resistance.

To provide the maximum power from the coil to the load, the maximum power transfer theory is applied. A compensating capacitor $C = 1/(\omega^2 L_{coil})$ is added in series to the coil to eliminate the coil inductance L_{coil}. The load resistance R_{load} should be the same of the coil resistance. Under this condition, as shown in Fig. 4, the power delivered to the load:

$$P_{load} = (\frac{V_{coil}}{2})^2/R_{coil} \qquad (3)$$

The power density of this system can be derived as follow:

$$D_{power} = \frac{1}{4}\frac{V_{coil}^2}{R_{coil}}/Vol \qquad (4)$$

where Vol is the total volume of the harvesting coil in m^3. To maximize the power output from the coil, its coil voltage V_{coil} should be increased while the coil resistance R_{coil} must be minimized. These two variables are correlated to the core shape, the core material and the properties of the enameled wires.

B. Optimum Core Shape Design

Since the harvesting coil cannot entirely enclose the power lines, the demagnetization phenomenon appears during the magnetization process, which decreases the effective
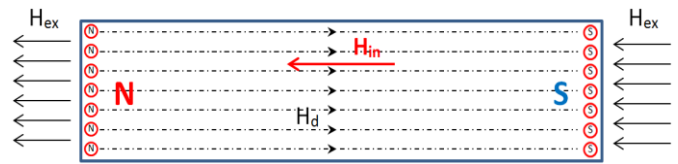

Fig. 6. The demagnetization field H_d inside a ferromagnetic bar when applying an external magnetic field H_{ex}
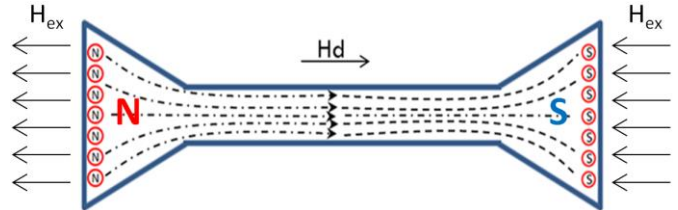

Fig. 7. The demagnetization field inside a bow-tie-shaped core when applying an external magnetic field

permeability μ_{eff}. When an external magnetic field H_{ex} is applied to the ferromagnetic rod/core as shown in Fig. 6, the north and south poles are created at two opposite sides, leading to the demagnetization field H_d.

$$H_{in} = H_{ex} - H_d \qquad (5)$$

The demagnetization field H_d depends on two factors [24]: the magnetization in the material (the surface pole strength) and the shape of the specimen (the pole distribution). The demagnetization factor D is introduced to describe the relationship between the demagnetization field H_d and the magnetization M.

$$H_d = D \times M \qquad (6)$$

The demagnetization factor D is solely determined by the specimen geometry [24]. Thus the core shape needs to be optimized to reduce the demagnetization factor. Roscoe et al used a solenoid with a ferromagnetic core to harvest the magnetic field energy in a substation [23]. They concluded that a thin long solenoid could have large effective permeability based on their experiment. However, a very long and thin solenoid may not be the best solution: although its volume may not be large, it can still occupy too much space because of its length. Furthermore, a long and thin ferromagnetic rod is brittle and prone to damage. We therefore propose a novel bow-tie-shaped core, shown in Fig. 7, which has a low demagnetization factor. The two ends of the core have been broadened like a bow-tie. There are two main reasons for choosing this shape to reduce the demagnetization factor:

1. Based on Gauss's Law for magnetism, the larger surface areas at the both ends can guide more magnetic flux from the air into the ferromagnetic core. This intensifies the magnetization at the middle of the core where the wire is wound on.

2. When this bow-tie core is magnetized, the south and north poles are mainly formed at the end surfaces. As the surface has been increased, the separation between the south and north poles is therefore increased, which results in a reduction of the demagnetization field at the middle of the bow-tie core.

To verify these two arguments, four cores depicted in Fig. 8 have been tested in the same uniform magnetic field generated by a Helmholtz coil. All of them have the following configurations for comparison:

1. The same length of 15 cm;

2. An ideal magnetic core material with the relative permeability μ_r and zero conductivity;

3. Winding numbers N=100 on the core;

4. Placed in the same alternating magnetic field area (6 μT_{rms}).

Solenoid (b), Dumbbell core (c) and Bow-tie core (d) have the same volume. The outer radius of Bow-tie core (d) equals to the radius of Solenoid (a). Dumbbell core (c) and Bow-tie core (d) have the same effective area that is orthogonal to the incoming magnetic field. Therefore, a fair comparison can be made to observe the effect on the different separations between the north poles and south poles. As the conductivity of the core material is intentionally set to zero, eddy currents can be eliminated inside the core. Therefore, we can focus on the magnetic properties with different core shapes. CST EM Studio is used as the simulation tool. A large Helmholtz coil is built to generate a uniform magnetic field area where the core under test is placed. The boundary condition is set to "open" to emulate the free space. Fig. 9 shows the simulated magnetic flux density B_{in} inside the four cores when the relative permeability μ_r is configured to 2000. The magnetic flux density B_{in}' at the middle is 785 μT_{rms} for Bow-tie core (d) and 633 μT_{rms} for Dumbbell core (c), but only 38.87 μT_{rms} for Solenoid (a) and 110 μT_{rms} for Solenoid (b). This validates the first argument that the large end surface (but small middle section) will increase the magnetization intensity in the middle of the core. The effective permeability μ_{eff}' and the fluxmetric demagnetization factor D' at the middle of the core can be

obtained using [24]:

$$\mu_{eff}' = B_{in}'/B_{ex} \qquad (7)$$
$$D' = (\mu_r/\mu_{eff}' - 1)/(\mu_r - 1) \qquad (8)$$

The fluxmetric demagnetization factors D' of Dumbbell core (c) and Bow-tie core (d) are found to be 0.009 and 0.007 respectively. The D' of Bow-tie core (d) is smaller than that of Dumbbell core (c), which validates the second argument that by increasing the separations between the north and south poles, the demagnetization factor can be reduced and therefore increase the power output.

It is also found that the effective permeability of Bow-tie core (d) is the highest among these four testing cores, as shown in Fig. 10. The μ_{eff}' of Solenoid (b) is 2 times bigger than that of Solenoid (a) which validates the concept discussed in [23]. Furthermore, four curves become saturated as μ_r increases. For the curves of Solenoid (a) and (b), their knee points appear when μ_r approaches 100. In contrast, for the curve of the bow-tie core, its knee point is around 300 and the effective permeability increased with μ_r, though the slope is small. However, the power density of the harvesting coil depends not only on μ_{eff}', but also on the effective cross section area and the coil resistance. As the ideal core material has been used, the coil resistance is determined by the copper resistance. If an enameled wire with the diameter of 0.14 mm and the resistivity of 1.11 Ω/m is used, the copper resistance is calculated and shown in Table I. According to Equations (3) and (4), the power
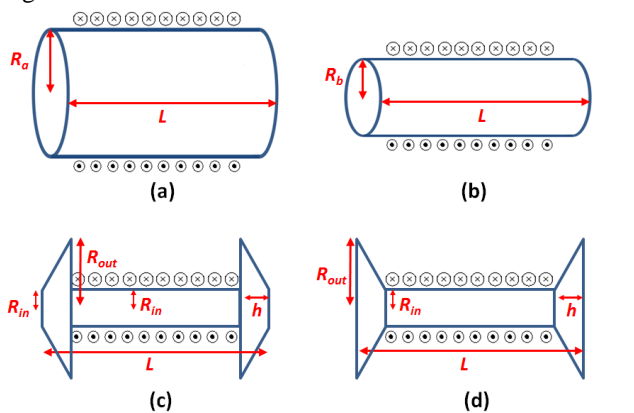

Fig. 8. (a) The conventional solenoid with R_a = 5 cm, L = 15 cm. (b) the conventional solenoid with R_b = 2 cm, L = 15 cm. (c) the dumbbell core with R_{out} = 5 cm, R_{in} = 1 cm, h = 2.4 cm and L = 15 cm. (d) the bow-tie core with R_{out} = 5 cm, R_{in} = 1 cm, h = 2.4 cm and L = 15 cm
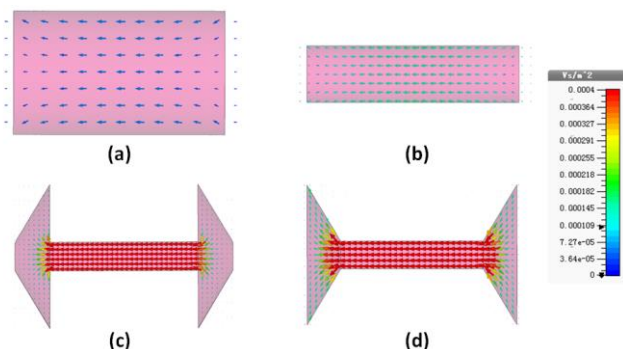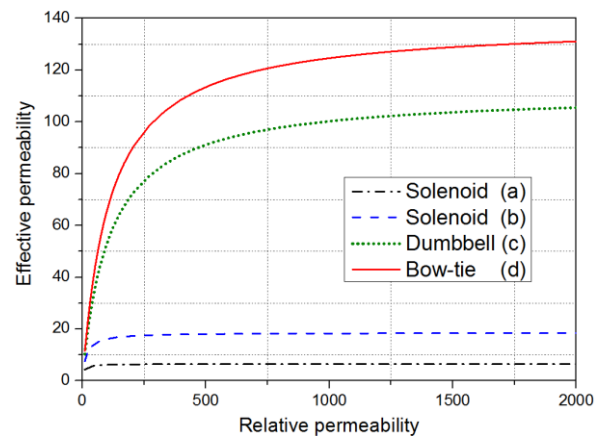

Fig. 9. The magnetic flux density B_{in} inside the four cores when the external magnetic density of 6 μT_{rms} is applied

Fig. 10. The effective permeability of three cores as a function of μ_r

TABLE I
THE PARAMETERS OF THE THREE CORES WHEN μ_R IS 2,000 AND N IS 100

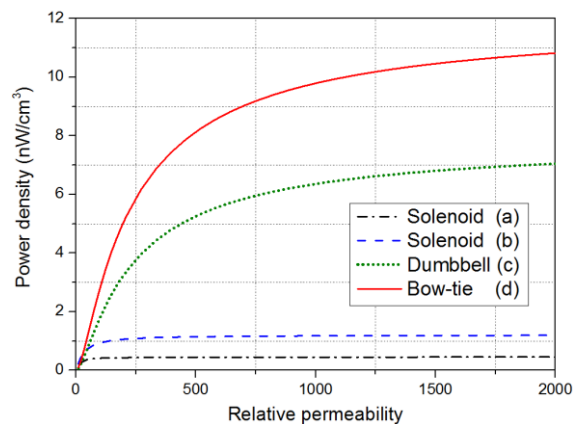| Core Type	Solenoid (a)	Solenoid (b)	Dumbbell (c)	Bow-tie (d)
Effective permeability	6.48	18.33	105.51	130.81
Demagnetization factor	0.154	0.0540	0.009	0.007
Open circuit voltage (mV$_{rms}$)	8.61	3.54	6.09	7.54
Wire resistance (Ω)	34.87	13.94	6.97	6.97
Output power (μW)	0.53	0.23	1.33	2.04
Power density (nW/cm^3)	0.45	1.19	7.04	10.82

Fig. 11. The power density of four cores as a function of μ_r when N is 100

density of the four cores is plotted in Fig. 11 as a function of the relative permeability μ_r. As shown in Table I, the bow-tie core has the smallest copper resistance due to its small inner radius R_{in}, which leads to the largest output power though its volume is much smaller than Solenoid (a). The output powers are low due to the small number of turns. The relationship between the winding properties and the output power will be discussed later. As shown in Fig. 11, when $\mu_r = 2000$, the power density of the Bow-tie core (d) is 1.5 times as much as that of Dumbbell core (c) and 8 times bigger than Solenoid (b). As a consequence, the bow-tie-shaped core shows the best performance compared with other cores.

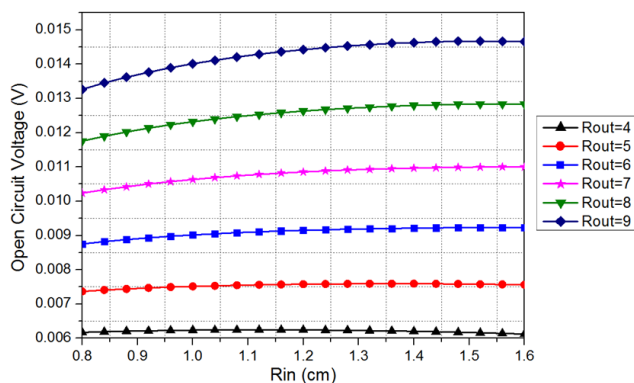A parametric study has been conducted on the bow-tie core

Fig. 12. The open circuit voltage of the bow-tie core with different inner radius R_{in} and outer radius R_{out}
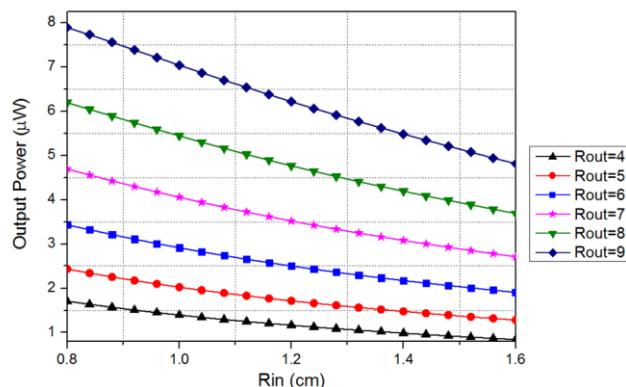

Fig. 13. The output power of the bow-tie core with different inner radius R_{in} and outer radius R_{out}

to maximize the output power when the volume and the length are fixed. The outer radius R_{out} and the inner radius R_{in} are tuned in a certain range, while the height h is configured accordingly to keep the core volume and length unchanged. In theory, when the outer radius R_{out} is increased, more magnetic flux can be guided into the core and the surface poles formed at the two ends are separated even further. Therefore, a larger outer radius may generate a higher voltage. Fig. 12 shows the simulation results. As the inner radius R_{in} increases, the coil voltage increases slightly. Nevertheless, a smaller inner radius will have lower copper resistance. When the outer radius R_{out} increases, the voltage increases significantly as shown in Fig. 12. As a consequence, a bow-tie core with a larger outer radius R_{out} and smaller inner radius R_{in} could have a higher power density as shown in Fig. 13.

C. Core Material Selection

It is important to note that the core material can have a huge effect on the performance of the harvesting coil. In [34], a research was conducted on harvesting magnetic field energy with different core materials. It was concluded that nanocrystalline alloy (FeSiB) was the most suitable material which has very high relative permeability (μ_r=8,000~40,000) and saturation magnetization. However, they did not consider the case that the harvesting coil could not entirely enclose the conducting current. As depicted in Fig. 10, due to the demagnetization factor, the effective permeability μ_{eff} becomes saturated when the relative permeability μ_r is higher than about 400. Therefore, ultra high μ_r would not provide a significant increment on the μ_{eff}. Instead, it is more important to focus on the reduction of the core losses. In general, the core losses can be divided into hysteresis losses and eddy current losses. By using the soft ferromagnetic material with low coercivity, the hysteresis losses in this application are considerably smaller than the eddy current losses due to the weak magnetic field and extremely low frequency. Roscoe et al used cast iron as the core material and the device suffered greatly from eddy current losses [23]. Their measurement results showed that the effective coil resistance was up to 33 kΩ, dominated by the eddy current losses. As a consequence, the eddy current must be minimized to maximize the power output delivered to the load. According to [24], the equation to calculate the power consumption of the eddy current losses is:

$$w_{eddy} = \frac{S}{2k\rho}(\frac{dB_{in}}{dt})^2 \qquad (9)$$

where S is the cross section in m²; B_{in} is the magnetic flux density inside the core in T; ρ is the material resistivity in Ω/m and k is the shape factor. We use stainless steel as the reference core material for the bow-tie coil shown in Fig. 8, whose relative permeability is close to 2,000 and conductivity is around 2.17 × 10⁶ S/m. Since the core material becomes conductive, eddy currents are generated when it is placed in an alternating magnetic field. The simulation indicates that the open circuit voltage is reduced to 5.9 mV compared with 7.6 mV when the conductivity is zero. Fig. 14(a) shows the eddy current density in the cross section at the middle of a bow-tie
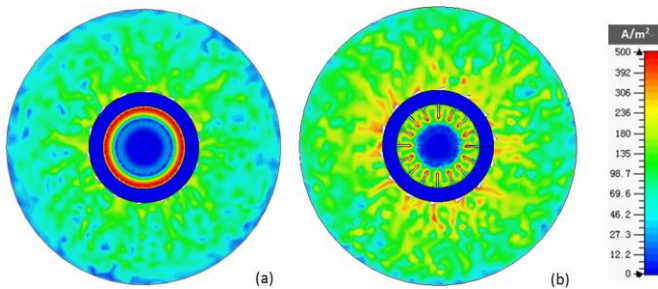
Fig. 14. The eddy current density inside the core when $\mu_r = 2,000$ and the conductivity $\sigma = 2.17 \times 10^6$ S/m: (a) The original core, (b) The core with air gaps
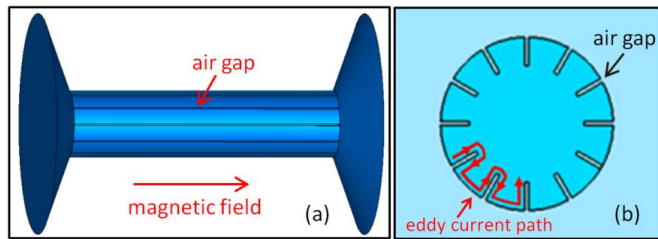

Fig. 15. The air gaps inside the bow-tie core: (a) External view, (b) Cross section view from the middle of the core

coil with $R_{out} = 5$ cm, $R_{in} = 1.5$ cm, $h = 1.4$ cm and $L = 15$ cm. At the edge of the core, the current density can be higher than 500 A/m^2. These eddy currents generate the magnetic field, which is against the external applied magnetic field.

To reduce the eddy current, the shape factor k was studied. Analogous to the core lamination used in the transformer, several air gaps have been introduced to the center rod as shown in Fig. 15. The simulation result depicted in Fig. 14(b) shows that the average current density inside the core is now reduced to 52 A/m^2. When more air gaps are introduced, the eddy current can be further reduced.

If only several air gaps are introduced, the eddy current is still significant. The material conductivity is investigated and Fig. 16 plots the complex open circuit voltage of the bow-tie coil as a function of the core conductivity. When the conductivity is zero, the open circuit voltage only contains imaginary part which represents the voltage that can be coupled to the load. When the conductivity increases from zero, the real part of the open circuit voltage appears caused by the eddy current losses inside the core, which is finally dissipated as heat. As the conductivity further increases, the real part can be higher than the imaginary part, which means most of the power is wasted in the core rather than delivered to the load. Thus we should have the conductivity as small as possible.
To summarize, the correct core material should have two main properties:

1. Soft ferromagnetic material with relative permeability above 400;

2. Minimal conductivity.

A ferrite seems to be the most suitable material according to these requirements. Mn-Zn soft ferrite could have relative permeability between 2,000 to 18,000 and ultra-low conductivity below 0.5 S/m [35]. In comparison, the conductivity of nanocrystalline alloy is normally higher than 7 $\times 10^5$ S/m. When a ferrite is used as the core material, the current density becomes several micro amperes per square
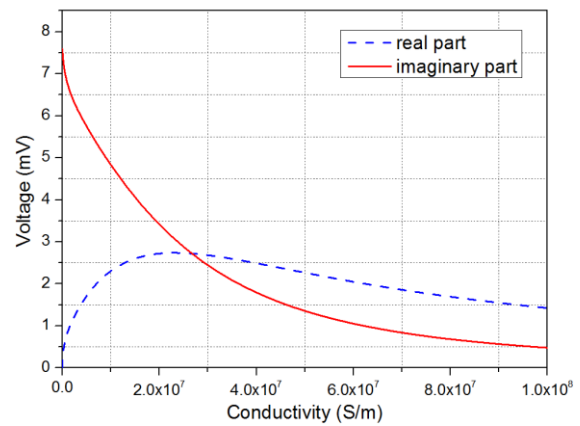

Fig. 16. The complex open circuit voltage of the bow-tie coil as a function of the core conductivity when the relative permeability is 2,000.
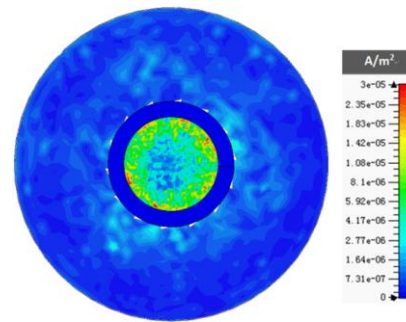

Fig. 17. The eddy current density inside the core with the relative permeability of 2000 and the conductivity of 0.35 S/m

meter in our case, as shown in Fig. 17. As a consequence, the eddy current is reduced significantly and the majority of the energy can be delivered to the load.

D. Power Output Calculation and Optimum Winding Method

The bow-tie coil can be treated as a solenoid with length L and radius r, leaving the average effective permeability μ_{eff} unchanged because the wires are only wrapped around the middle part of the core as shown in Fig. 18. The open circuit voltage can be obtained by applying Faraday's Law:

$$V_{coil} = N\pi r^2 \omega \mu_{eff} B_{ex} \qquad (10)$$

The equivalent coil resistance R_{coil} can be divided into copper losses and core losses:

$$R_{coil} = R_{copper} + R_{core} \qquad (11)$$

As the ferrite is selected as the core material, the core losses are considerably smaller compared with the copper losses when the number of winding turns N is sufficiently large:
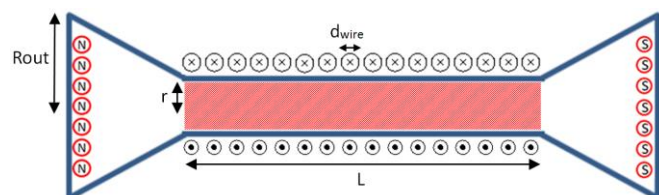
$$R_{coil} \approx R_{copper} \qquad (12)$$

Fig. 18. The physical dimensions of the bow-tie coil. *Rout* and *r* is the outer and inner radius. d_{wire} indicates the diameter of the enameled wires winding on the core. *L* represents the length of the center rod around which the wires are wrapped.

There should be several layers of the enameled wire wrapped around the core as a large number of winding turns are needed to acquire a high coil voltage.

$$K_{layer} = N/(L/d_{wire}) \qquad (13)$$

The total length l_{wire} of the enameled wire can be obtained as a function of the number of turns N:

$$l_{wire} = (\frac{r + r + K_{layer} \times d_{wire}}{2})2\pi N \qquad (14)$$

Using Equations (2), (11) and (12), the copper resistance can be derived as:

$$R_{copper} = 2\pi r N\rho + \pi N^2 d_{wire}{}^2 \rho/L \qquad (15)$$

According to (10) and (15), the power delivered to the matched load can be obtained as:

$$P_{load} = N\pi(r^2 \omega\mu_{eff} B_{ex})^2 / \left(8r\rho + \frac{4\rho N d_{wire}{}^2}{L}\right) \qquad (16)$$

The power output is dependent upon the property of the enameled wires in addition to the core shape and material. A higher winding number N could generate a higher voltage but could also produce a larger copper resistance. The enameled wire with a larger diameter has lower resistivity but occupies more space. The properties of the enameled wire should be fully investigated to boost the power output from the coil.

Firstly, the enameled wire with the fixed diameter of 0.14 mm and the resistivity of 1.11 Ω/m is wound on two ferrite cores with the same dimensions shown in Fig. 8(b, d). The
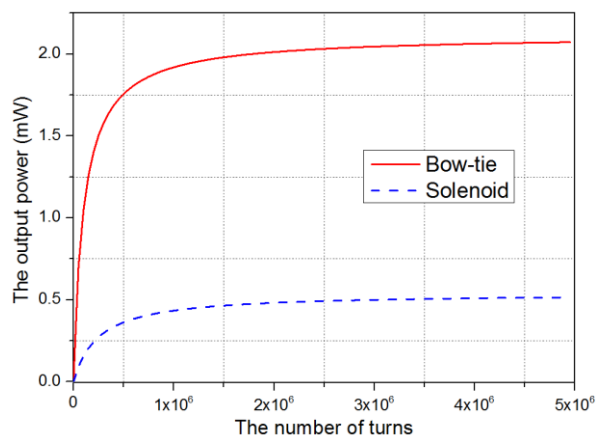

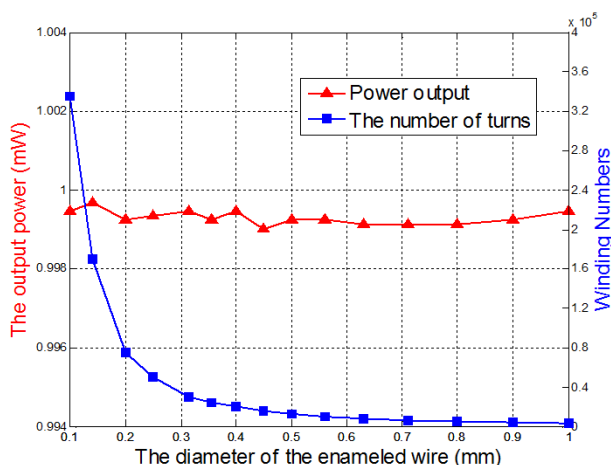Fig. 19. The power output as a function of the winding number

Fig. 20. The power output of the bow-tie coil when different wires are used

power output is plotted in Fig. 19 as a function of the winding number, which indicates that the power output of the two coils increases with the increment of the winding number. However, when the number of turns is extremely large, the power becomes saturated as there are too many layers on the core. In this situation, each turn added on the core requires much longer wires and results in larger resistance. In practical, it is impossible to wound 1,000,000 turns of enameled wire on such a small coil.

Secondly, by giving a fixed space of $8 \times 10^{-4}\,\mathrm{m}^3$, the wires with different diameters [36] are fully wound on the bow-tie core and their corresponding power output is plotted in Fig. 20. As the diameter increases, the number of turns decreases due to the fixed space while the power output does not change significantly. Therefore, the output power from the coil does not depend on the type of the enameled wire used but depends on the volume that the enameled wire occupies. From the financial point of view, the wire with a larger diameter is preferred as its unit price is cheaper. From the power delivery point of view, the enameled wire with a smaller diameter is better which can obtain a higher winding number and result in a higher coil voltage. When the coil is connected to a rectifier circuit, high coil voltage could lower the power dissipation on the rectifying diode, which increases the power transfer efficiency.

In conclusion, to increase the output power from the energy harvesting system, thin wires are preferred and the number of winding turns should be as large as possible.

IV. EXPERIMENT VALIDATIONS AND RESULTS

A Helmholtz coil (consisting of two identical coil rings) is made to generate a uniform magnetic field to imitate the environment under overhead power lines. The diameter of each coil ring is 1 meter with 33 turns of conducting wire on it and the two coil rings are separated by half a meter. With a 120 mA$_{rms}$ current passing through the Helmholtz coil, a magnetic flux density of 7 μT$_{rms}$ is generated. A bow-tie coil and a
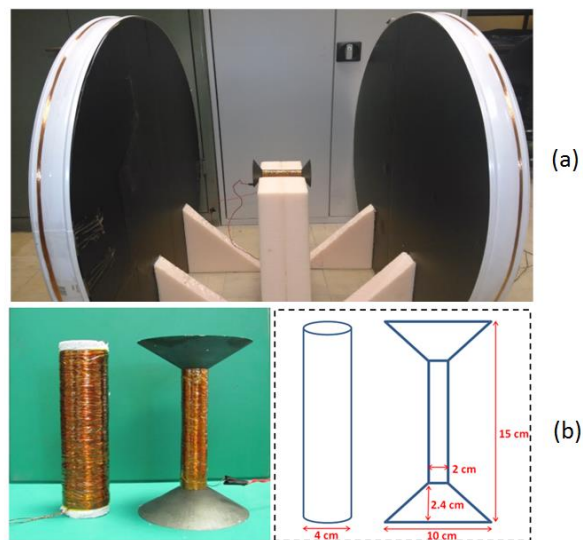

Fig. 21. (a) A Helmholtz coil used to generate a uniform magnetic flux density in the laboratory, (b) The solenoid and the bow-tie coil made by ferrite with the given dimension

solenoid with the same volume and length are fabricated. The specimens and their dimensions are shown in the Fig. 21(b). Mn-Zn ferrite [37] is used as the core material with relative permeability 2300 $\pm$ 25% and conductivity of 0.154 S/m. Two coils are put into the Helmholtz coil and their open circuit voltages are measured using a multimeter. The results are compared against the simulated ones as shown in Fig. 22. From the measurement results, the voltage of the bow-tie coil is 1.5 times of that of the solenoid. This validates the concepts discussed in the previous section. It is noted that the simulation results are higher than the experiment values. This should be mainly caused by the errors in the fabricated ferrite core. First, the relative permeability of the ferrite is in the range of 1700 to 2900 according to the datasheet [37], which may bring some uncertainty into the experiment. Secondly, due to the special geometry of the bow-tie coil, it is difficult and expensive to manufacture this whole ferrite core in one piece. Instead, five pieces are fabricated and then glued together as shown in Fig. 23. Therefore, gaps may exist in each contact surface. In this situation, the magnetic flux in the core and the effective permeability are reduced because more energy is required to drive the same flux across the air gap than through an equal volume of the ferrite [24]. As the air gap increases, the effective permeability will be further reduced. When a 0.05 mm air gap is introduced, the simulation results show that the average effective permeability decreases from 128 to 108 and its corresponding coil voltages are close to the measured values.

The effective coil resistance can be measured by a 50 Hz bridge. The power output at the load can be maximized by tuning the capacitor and the load resistance. In this situation, based on the maximum power transfer theory, the effective coil resistance should be the same as the load resistance. The copper resistance is measured with a multi-meter and results are included in Table II. They indicate the copper resistance

dominates the effective coil resistance, proving that the eddy current losses are minimized. The measurement results are then compared to the theoretical values as shown in Fig. 24.

For the same winding numbers, the copper resistance of the bow-tie coil is smaller than that of the solenoid. As for this novel bow-tie coil, the copper wire is wound around its middle part where the radius is small. Hence, the same number of turns can be achieved with a short enameled wire which results in a smaller copper resistance. The measured values are higher than the theoretical values. Since the two coils are not wound by a fully automatic coil winding machine due to the requirement of special fixtures. Therefore windings are not perfectly aligned which causes a longer wire to achieve the same number of turns and results in the difference between the measured and theoretical values. To wind 40,000 turns on the bow-tie core shown in Fig. 21(b), in the ideal situation when the enameled wire is perfectly aligned, the winding diameter shown in Fig. 25 would be 4.74 cm. However, the measurement result is 5.5 cm which means a longer wire was used in practice.

When the air gap model is used to describe the coil voltage, the theoretical values align with the experiment results. The measurement results indicate that the power output from the

TABLE II
THE MEASUREMENT RESULTS OF THE EFFECTIVE COIL RESISTANCE

Coil Type	Windings	R-wire (kΩ)	R-coil (kΩ)
Solenoid	8,000	1.69	1.70
Bow-tie Coil	8,000	1.09	1.2
Solenoid	24,000	5.28	5.25
Bow-tie Coil	24,000	3.72	3.66
Solenoid	40,000	8.63	8.78
Bow-tie Coil	40,000	5.95	6.03

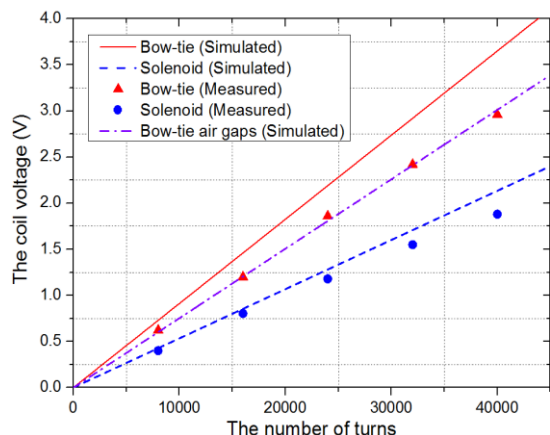Fig. 24. The copper resistance of the two coils as a function of the winding numbers.

Fig. 22. The measurement results of the open circuit voltage as a function of the winding numbers.
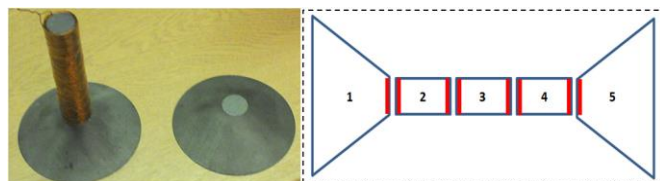
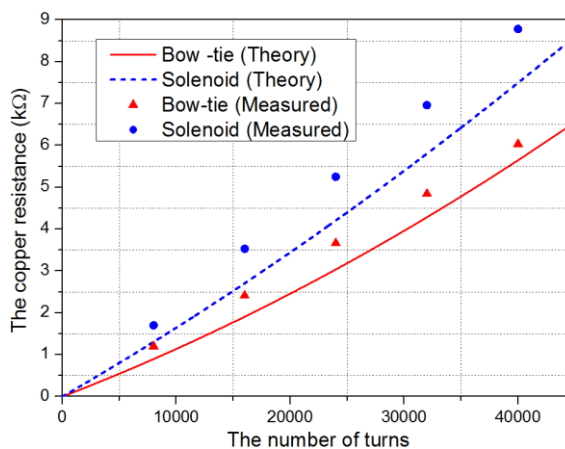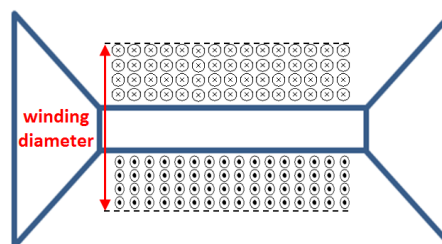Fig. 23. The bow-tie coil fabricated in 5 small piece and then glued together

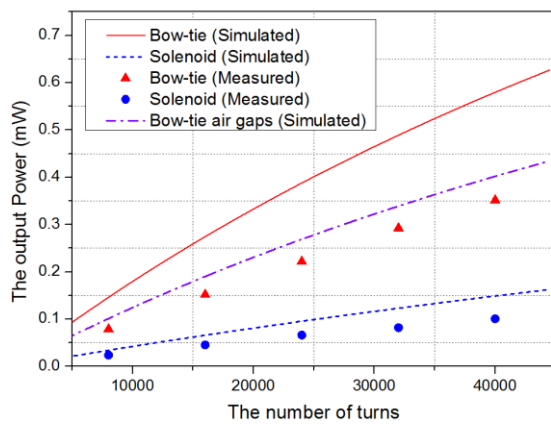Fig. 25. The winding diameter of a bow-tie coil

Fig. 26. The power output of the two coils as a function of the winding numbers.

TABLE III
THE MEASUREMENT RESULTS OF THE COIL OUTPUT WITH DIFFERENT WIRES

Wire Type	0.14 mm	0.49 mm	1.00 mm
Resistivity (Ω/m)	54.41	2.176	0.544
Number of turns	103,060	9,500	2,430
Coil voltage (V_{rms})	8.36	0.730	0.181
Coil resistance (Ω)	21500	160.2	10.1
Power (mW)	0.8127	0.831	0.811

bow-tie coil can be 2.5 times greater than the output from the conventional solenoid with 40,000 turns. In this case, the power density of the bow-tie coil is 1.86 $\mu W/cm^3$ compared to 0.53 $\mu W/cm^3$ from the solenoid when placed in a magnetic flux density of 7 μT_{rms}

For a fixed space of 8×10^{-4} m^3, three different enameled wires have been selected to fully wind on the bow-tie core. Their parameters and output powers are shown in Table III. As expected, the output power does not change much for different wires although other parameters are changed significantly in Table III.

V. DISCUSSIONS AND POTENTIAL APPLICATIONS

From the experiment, 360 μW was collected at the load by using the bow-tie coil with 40,000 turns, which might be enough to power a small wireless sensor [38]. To boost the power output from the coil for energy hungry sensors, three methods have been considered:

1. To increase the length and the outer radius of the bow-tie coil to increase the effective permeability.

2. To put the coil closer to the power line to increase the external magnetic flux density.

3. To increase the number of winding turns.

If the length and the outer radius of the bow-tie coil can be made larger as shown in Fig. 27, the average effective permeability can be increased from 128 to 615. If we wind 160,000 turns of enameled wires with the diameter of 0.14 mm on the core and place the coil 5 meters above the ground where the magnetic flux density is typically around 11 μT, in this situation, the estimated output power is around 146.7 mW which gives the estimated power density of 103.5 $\mu W/cm^3$. This value is comparable to the solar panel working during a
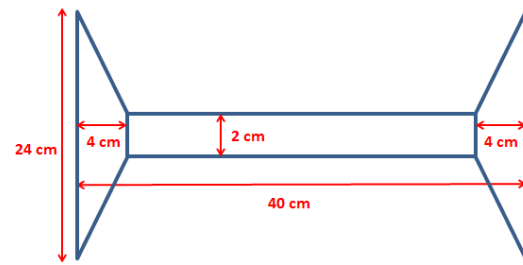

Fig. 27. The bow-tie coil with longer length and larger outer radius
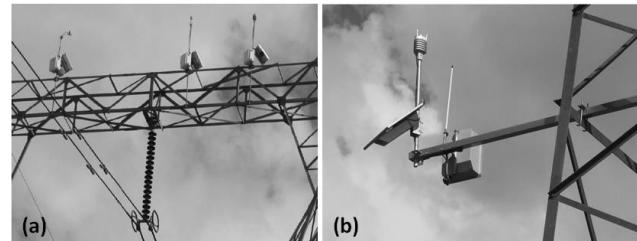

Fig. 28. Installation of weather stations on a pylon [40]. (a). on the top of the pylon. (b) on the anti-climbing protective device

cloudy day [15], but the solar panel does not work at night unlike the proposed solution.

The power consumption of a typical weather station [20] and a GPRS data logger [39] is 36 mW and 3.6W respectively. If the weather station collects the data in every 30 minutes and the data logger takes a maximum of 1 minute to transmit the information to the server, the average power consumption would be 120 mW. The dynamic thermal rating [40, 41] suggested the weather station should be installed either on top of the pylon or on the anti-climbing protective device as shown in Fig. 28. In both situations, the height to the ground is larger than 5 meters. This means that the large bow-tie coil shown in Fig. 27 is able to power the weather station and the data logger.

The bow-tie coil proposed in this paper is compared with other recently reported designs. Roscoe *et al* designed a 50 cm long solenoid with the diameter of 5 cm to collect the magnetic field energy in a substation [23]. The power density of their coil was only 0.845 $\mu W/cm^3$ when it was placed in a magnetic flux density of 18.5 μT_{rms}. If the bow-tie coil designed in this paper was placed in the same magnetic flux density with the same winding number, the power density would be 13.0 $\mu W/cm^3$, which is 15 times more than their design. In addition, their coil is longer and bigger than our bow-tie coil.

VI. CONCLUSIONS

In this paper, a new and efficient harvesting coil to scavenge the magnetic field energy under overhead power lines has been proposed and presented. The coil does need to be clamped to the power line and can be placed just above the ground, thus sensors with a larger volume can be powered which is impossible for the conventional method of mounting the energy harvester on the power lines.

A novel bow-tie coil has been introduced, designed and optimized to produce a much higher power density (1.86 $\mu W/cm^3$) than the conventional solenoid design (0.53 $\mu W/cm^3$). This was based on the theoretical analysis and subsequently verified by the experiment measurements. The special design of

its geometric shape and a good selection of the core material have led to much greater effective permeability and lower loss resistance. The core material was selected specifically to eliminate eddy current losses. Ferrite was identified as the most suitable core material, given its high relative permeability and ultra-low conductivity. Different winding methods have been investigated. The results indicated that the power collected by the coil was not only determined by the types of the enameled wire, but also proportional to volume that the wire occupied. However, the wire with a smaller diameter can have higher energy transfer efficiency. It was demonstrated that the power density of the bow-tie coil designed in this paper was 15 times greater than a recently reported result if both coils were placed into the same magnetic field (our coil was smaller). Thus the proposed solution is extremely effective and flexible on harvesting energy under the overhead power lines and can be used to power a range of sensors.

REFERENCES

[1]   M. Lacroix, L. Brouillette, and A. Blais, "Hydro Quebec's de-icing system: Automated overhead line monitoring and de-iceing system", in *Proc.CIFRE*, 2008, pp. B2–211.

[2]   K. Savadjiev and M. Farazaneh, "Modeling of icing and ice shedding onoverhead power lines based on statistical analysis of meteorological data", *IEEE Transactions on Power Delivery*, Vol. 19, No. 2, 2004, pp. 715–722,

[3]   H. Zangl, T. Bretterklieber and G. Brasseur, "A Feasibility Study on Autonomous Online Condition Monitoring of High-Voltage Overhead Power Lines", *IEEE Transactions on Instrumentation and Measurement,* Vol. 50, No. 5, 2009, pp. 1789-1796

[4]   V. Raghunathan, A. Kansal, J. Hsu, J. Friedman, Mani Srivastava, "Design considerations for solar energy harvesting wireless embedded systems," *Information Processing in Sensor Networks,* 2005, pp. 457-462

[5]   S. Bader, B. Oelmann, "Enabling Battery-Less Wireless Sensor Operation Using Solar Energy Harvesting at Locations with Limited Solar Radiation," *4th Int. conf. on Sensor Technologies and Applications (SENSORCOMM),* 2010, pp. 602-608

[6]   J. A. Paradiso and T. Starner, "Energy Scavenging for Mobile and Wireless Electronics", *IEEE Pervasive Computing*, Vol. 4, 2005, pp.18-27

[7]   C. Tsai, C. Hsieh, S. Huang, "Enhancement of Damage-Detection of Wind Turbine Blades Via CWT-Based Approaches", *IEEE Transactions on Energy Conversion,* Vol. 21, No. 3, 2006, pp. 776-781.

[8]   K. Chang, S. Kang, K. Park and S. Shin, "Electric Field Energy Harvesting Powered Wireless Sensors for Smart Grid", *Journal of Electrical Engineering & Technology,* Vol. 7, No. 1, 2012, pp. 75~80

[9]   T. Keutel, X. Zhao and O. Kanoun, "Energy Scavenging for Monitoring of Overhead Power Line Networks", in *Proc. IMTC*, 2009,pp. 207-211

[10] M. J. Moser, T. Bretterklieber, H. Zangl and G. Brasseur, "Strong and Weak Electric Field Interfering: Capacitive Icing Detection and Capacitive Energy Harvesting on a 220-kV High-Voltage Overhead Power Line", *IEEE Transaction on Industrial Electronics*, Vol. 58, No. 7, 2011, pp. 2597-2604

[11] F. Guo, H. Hayat, and J. Wang, "Energy Harvesting Devices for High Voltage Transmission Line Monitoring", *Power and Energy Society General Meeting*, July, 2011, pp. 1-8

[12] X. Zhao, T. Keutel and M. Balduaf, "Energy harvesting for a wireless-monitoring system of overhead high-voltage power lines", *IET Generation, Transmission & Distribution*, Vol. 7, Issue: 2, 2013, pp. 101-107

[13] J. Moon, S.B. Leeb, "Analysis Model for Magnetic Energy Harvesters", *IEEE Transactions of Power Electronics*, Vol.30, Issue: 8, 2015, pp. 4302-4311

[14] R. Moghe, D. Divan, F. Lambert, "Powering Low-Cost Utility Sensors using Energy Harvesting", *Power Electronics and Applications (EPE 2011)*, in *Proc. 2011-14th European Conference*, 2011, pp. 1-10

[15] K. Tashiro, H. Wakiwaka, S. Inoue, and Y. Uchiyama, "Energy Harvesting of Magnetic Power-Line Noise", *IEEE Transactions on Magnetics*, Vol. 47, Issue: 10, 2011, pp. 4441-4444

[16] J.P. Amaro, "Energy harvesting for Zigbee compliant Wireless Sensor Network nodes", *IECON 2012 - 38th Annual Conference on IEEE Industrial Electronics Society*, 2012, pp. 2583-2588

[17] T. Taithongchai and Ekachai, "Adaptive Electromagnetic Energy Harvesting Circuit for Wireless Sensor Application", *Electrical Engineering/Electronics, Computer, Telecommunications and Information Technology*, 2009, pp. 278-281

[18] C. Li, G. Ma and B. Qi, "Condition Monitoring and Diagnosis of High-Voltage Equipment in China –Recent Progress", *IEEE Electrical Insulation Magazine*, Vol. 29, Issue: 5, 2013, pp. 71-78

[19] D.M. Green, J.P. Gentle and K.S. Myers, "A Comparison of Real-Time Thermal Rating Systems in the U.S. and the U.K.", *IEEE Transactions on Power Delivery*, Vol. 29, Issue: 4, 2014, pp. 1849-1858

[20] Vaisala, Vaisala Weather Transmitter WXT520 Access to Real Time Weather Data, http://www.vaisala.com/Vaisala%20Documents/Brochures%20and%20 Datasheets/WEA-MET-WXT520-Weather-datasheet-B210417EN-K-L OW.pdf

[21] M. Zhu and M.D. Judd, "Energy Harvesting in Substations for Powering Autonomous Sensors", *Third International Conference on Sensor Technologies and Applications*, 2009, pp. 246-251

[22] M. Zhu and P.C. Baker, "Alternative Power Sources for Autonomous Sensors in High Voltage Plant", *2009 IEEE Electrical Insulation Conference*, 2009, pp. 36-40

[23] N. M. Roscoe and M. D. Judd, "Harvesting Energy from Magnetic Fields to Power Condition Monitoring Sensors", *IEEE Sensors Journal*, Vol. 13, Issue: 6, 2013, pp. 2263-2270

[24] D. Jiles, "Introduction to Magnetism and Magnetics Materials", in *Magnetism*, 2nd ed. Ames, Iowa: Chapman & Hall, 1998, pp. 49-51

[25] B. Zemljaric, "Calculation of the Connected Magnetic and Electric Fields Around an Overhead-Line Tower for an Estimation of Their Influence on Maintenance Personnel", *IEEE Transactions on Power Delivery* , Vol. 26, No. 1, 2011, pp.467-474

[26] D. Andreuccetti, N. Zoppetti, R. Conti, N. Fanelli, A. Giorgi and R. Rendina, "Magnetic Fields from Overhead Power Lines: Advanced Prediction Techniques for Environmental Impact Assessment and Support to Design ",in *Proc.BPTCP*, 2003,

[27] A.R. Memari and W. Janischewskyj, "Mitigation of Magnetic Field Near Power Lines", *IEEE Transactions on Power Delivery*, Vol.11, NO.3, July 1996, pp.1577-1586

[28] B.J. Maddock, "Overhead line design in relation to electric and magnetic field limits", *Power Engineering Journal*, Vol. 6, Issue:5, 1992, pp. 217-224

[29] National Grid, EMF.info Electric and Magnetic Field, http://www.emfs.info/sources/overhead/factors/height/

[30] W. He, B. Wan, C. Pei, J. Zhang and J. He, "Effect of Humidity on Transmission Lines' Power Frequency Electric Field Measurements", *Asia-Pacific Symposium on Electromagnetic Compatibility*, 2012, pp.289-292

[31] A. Dein, "Magnetic-Field Calculation Under EHV Transmission Lines for More Realistic Cases", *IEEE Transactions on Power Delivery*, Vol. 24, No. 4, 2009, pp.2214-2222

[32] A.E. Tzinevrakis, D.K. Tsanakas, E.I. Mimos, "Electric field analytical formulas for single-circuit power lines with a horizontal arrangement of conductors", *IET Generation, Transmission & Distribution*, Vol. 3, Issue: 6, 2009, pp.509-520.

[33] A.E. Tzinevrakis, D.K. Tsanakas, E.I. Mimos, "Analytical Calculation of the Electric Field Produced by Single-Circuit Power Lines", *IEEE Transactions on Power Delivery*, Vol. 23, No. 3, 2008, pp. 1495-1505.

[34] M.P. dos Santos, D.A. Vieira and Y.P.M. Rodriguez, "Energy harvesting using magnetic induction considering different coil material ", in *Proc. I2MTC*, 2014

[35] Ferroxcube soft Mn-Zn ferrite cores, datasheet available at http://www.ferroxcube.com/FerroxcubeCorporateReception/datasheet/sfe misup.pdf

[36] Enameled wires, Data Table for Solid Round Wire, http://www.williamsonic.com/WireTable/index.html

[37] Mn-Zn ferrite, DMR40 Material Characteristics, http://www.italtras.us/PDF/SCHEDA%20TECNICA%20EE32%20in%20DMR40.pdf

[38] MICAz wireless sensor, (MPR2400) 2.4 GHz Mote, http://www.memsic.com/products/wireless-sensor-networks/wirelessmodules.html,

[39] Invisible-systems, Gateway GPRS, GPS & RF, http://www.invisible-systems.com/solutions/pdf/Gateway%20GPS%20RF.pdf

[40] D. J. Spoor and J. P. Roberts, "Development and Experimental Validation of a Weather-Based Dynamic Line Rating System", *IEEE Innovative Smart Grid Technologies Asia (ISGT), 2011,* pp. 1-7.

[41] M. Matus, D. Saez and M. Favley, "Identification of Critical Spans for Monitoring Systems in Dynamic Thermal Rating", *IEEE Transactions on Power Delivery,* Vol. 27, No. 2, 2012, pp. 1002-1009

Sheng Yuan was born in Shanghai, China, in 1990. He received the B.Eng degree (first class) in microelectronics and telecommunication engineering from Xi'an Jiao Tong Liverpool University, Suzhou, China and the University of Liverpool, Liverpool, United Kingdom, in 2012. He is currently working toward the Ph.D. degree at the University of Liverpool, UK.

His research interests include indoor navigation and position system, wireless energy harvesting, power management circuit, wireless power transfer, and RFID.

Yi Huang (S'91–M'96–SM'06) received B.Sc. degree in physics from Wuhan University, China, the M.Sc. (Eng.) degree in microwave engineering from NRIET, Nanjing, China, and the D.Phil. degree in communications from the University of Oxford, Oxford, U.K., in 1994.

He has been conducting research in the areas of wireless communications, applied electromagnetics, radar and antennas for the past 25 years. His experience includes 3 years spent with NRIET (China) as a Radar Engineer and various periods with the Universities of Birmingham, Oxford, and Essex, in the U.K., as a member of research staff. He worked as a Research Fellow at British Telecom Labs in 1994, and then joined the Department of Electrical Engineering & Electronics, the University of Liverpool, U.K., as a Faculty member in 1995, where he is now a Full Professor in Wireless Engineering, the Head of High Frequency Engineering Research Group, and M.Sc. Programme Director. He has published over 200 refereed papers in leading international journals and conference proceedings, and is the principal author of the popular book Antennas: from Theory to Practice (Wiley, 2008). He has received many research grants from research councils, government agencies, charity, EU, and industry, acted as a consultant to various companies, and served on a number of national and international technical committees.

Prof. Huang has been an Editor, Associate Editor, or Guest Editor of four of international journals. He has been a keynote/invited speaker and organiser of many conferences and workshops (e.g., IEEE iWAT 2010, WiCom 2006, 2010, and LAPC2012). He is at present the Editor-in-Chief of Wireless Engineering and Technology, a UK National Rep of European COST-IC1102, an Executive Committee Member of the *IET Electromagnetics PN*, and a Fellow of IET, U.K

Jiafeng Zhou received the B.Sc. degree in radio physics from Nanjing University, Nanjing, China, in 1997, and the Ph.D. degree from the University of Birmingham, Birmingham, U.K., in 2004. His doctoral research concerned high-temperature superconductor microwave filters.

From July 1997, for two and a half years he was with the National Meteorological Satellite Centre of China, Beijing, China, where he was involved with the development of communication systems for Chinese geostationary meteorological satellites. From August 2004 to April 2006, he was a Research Fellow with the University of Birmingham, where his research concerned phased arrays for reflector observing systems. Then he moved to the Department of Electronic and Electrical Engineering, University of Bristol, Bristol, U.K until August 2013. His research in Bristol was on the development of highly efficient and linear amplifiers. He is now with the Department of Electrical Engineering and Electronics, University of Liverpool, Liverpool, UK. His current research interests include microwave power amplifiers, filters, electromagnetic energy harvesting and wireless energy transfer

Qian Xu received the B.Eng. and M.Eng. degrees from the School of Electronics and Information, Northwestern Polytechnical University, Xi'an, China, in 2007 and 2010. He is currently working towards the Ph.D. degree in electrical engineering at the University of Liverpool, U.K.

He worked as a RF engineer in Nanjing, China in 2011 and an Application Engineer in CST, Shanghai, China in 2012. His current research interests include computational electromagnetics, reverberation chamber and anechoic chamber.

Chaoyun Song was born in Gansu, China, in 1990. He received the B.Eng degree (Hons) in telecommunication engineering from Xi'an Jiao Tong Liverpool University, Suzhou, China, in 2012 and the M.Sc. degree with distinction in microelectronics and telecommunication from the University of Liverpool, Liverpool, United Kingdom, in 2013. He is currently working toward the Ph.D. degree at the University of Liverpool, Liverpool, UK.

His research interests include antenna design, power management circuit, wireless power transfer and energy harvesting, and wearable antennas

Pete Thompson is the Managing Director of Invisible-Systems Ltd, a dynamic and innovative company that designs, manufactures and supplies a wide range of wireless monitoring systems for a variety of applications. With more than 15 years of experience in the wireless condition and energy monitoring/reduction, he founded Invisible-System Ltd to provide effective solutions for both private and public organizations to improve the energy efficiency, reduce the carbon output and the utility cost. The vision for Invisible Systems was originally to provide a wireless system that was easy to install and 'general purpose' to monitor and control be suited to a wide range of applications, including energy and condition monitoring.

The concept is a 'total solution' including hardware and web software (Realtime Online), applications range from monitoring critical assets such as HV transformers on sub stations to fridges in high street retail shops. The product is totally wireless with local RF communications to a cellular gateway therefore avoiding any on-site IT infrastructure. Invisible Systems employ 12 x R&D engineers support the design and development of the product.